
4-Step Renal Dosimetry Dependent on Cortex Geometry Applied to ^{90}Y Peptide Receptor Radiotherapy: Evaluation Using a Fillable Kidney Phantom Imaged by ^{90}Y PET

Stephan Walrand, François Jamar, Larry van Elmbt, Renaud Lhommel, Edgar Bidja'a Bekonde, and Stanislas Pauwels

Nuclear Medicine Center, Université Catholique de Louvain, Brussels, Belgium

Accurate dosimetry in ^{90}Y peptide receptor radionuclide therapy (PRRT) helps to optimize the injected activity, to prevent kidney or red marrow toxicity, while giving the highest absorbed dose to tumors. The aim of this study was to evaluate whether direct ^{90}Y bismuth germanate or lutetium yttrium orthosilicate time-of-flight PET was accurate enough to provide dosimetry estimates suitable to ^{90}Y PRRT. **Method:** To overcome the statistical uncertainty arising from the low ^{90}Y positron counting rate, the computation of the cortex mean-absorbed dose was divided into 4 steps: delineation of the cortex volume of interest (VOI) on the CT scan, determination of the recovery coefficient from the cortex VOI using the point-spread function of the whole imaging process, determination of the mean cortex-absorbed dose per unit cumulated activity in the cortex ($S_{\text{cortex} \leftarrow \text{cortex}}$ value) from the cortex VOI using a ^{90}Y voxel S value kernel, and determination of the number of decays in the cortex VOI from the PET reconstruction. Our 4-step method was evaluated using an anthropomorphic abdominal phantom containing a fillable kidney phantom based on the MIRD kidney model. Vertebrae with an attenuation similar to that of bone were also modeled. Two tumors were modeled by 7-mL hollow acrylic spheres and the spleen by a plastic bag. Activities corresponded to typical tissue uptake in a first ^{90}Y -DOTATOC cycle of 4.4 GBq, considered as free of significant renal toxicity. Eight successive 45-min scans were acquired on both systems. **Results:** Both PET systems were successful in determining absorbed dose to modeled tumors but failed to provide accurate red marrow dosimetry. Renal cortex dosimetry was reproducible for both PET systems, with an accuracy of 3% for the bismuth germanate system but only 18% for the lutetium yttrium orthosilicate time-of-flight system, which was hindered by the natural radioactivity of the crystal, especially in the most attenuated area of the kidney. **Conclusion:** This study supports the use of direct ^{90}Y PET of the first PRRT cycle to assess the kidney-absorbed dose and optimize the injected activity of the following cycles.

Key Words: PET/CT; radiobiology/dosimetry; radionuclide therapy; PET; PRRT; dosimetry; kidney; ^{90}Y

J Nucl Med 2010; 51:1969–1973

DOI: 10.2967/jnumed.110.080093

Received Jun. 9, 2010; revision accepted Sep. 15, 2010.
For correspondence or reprints contact: Stephan Walrand, Médecine Nucléaire, Av Hippocrate 10, 1200 Brussels, Belgium.
E-mail: stephan.walrand@uclouvain.be
COPYRIGHT © 2010 by the Society of Nuclear Medicine, Inc.

Peptide receptor radionuclide therapy (PRRT) with ^{90}Y is widely used for internal radiotherapy of neuroendocrine tumors (1). ^{90}Y has a long β^- range that, although suboptimal for small tumors, irradiates rather uniformly larger tumors that often display heterogeneous perfusion. This irradiation ability was confirmed in an animal model, in which a combination of ^{90}Y - and ^{177}Lu -labeled somatostatin analog showed a better tumor response than either radioisotope alone (2). Used alone, ^{90}Y PRRT is frequently administered in several cycles. The dose fractionation has proven less toxic for the kidney (3) because it allows DNA repair in normal tissues between cycles, without a noticeable reduction of the tumor response (4).

Assessment of the absorbed doses in the target and critical tissues is also needed to optimize the activity to inject (5–9). Until recently, investigators focused on the major emission of ^{90}Y (i.e., β -rays) that was imaged with SPECT using the bremsstrahlung x-rays, the energy spectrum of which is continuous. Despite recent correction methods (10), ^{90}Y SPECT still suffers from a relatively poor spatial resolution and inaccurate quantification. ^{87}Y (93%, 485 keV; 100%, 389 keV) was theoretically investigated for SPECT (11) but rarely used because of the potential toxicity of its daughter element, $^{87\text{m}}\text{Sr}$. ^{86}Y PET was developed during the last decade, providing probative results in dosimetry assessment (3,4) and the same dose-toxicity response for the kidney as that provided by external-beam radiotherapy (12). However, radiopharmaceutical-grade ^{86}Y is not commercially available and requires a 16-MeV cyclotron for its production. Furthermore, its high abundance of prompt single γ -rays involves sophisticated correction methods for accurate quantification (13). As a result, these methods cannot be widely used in clinical practice.

An ^{111}In -labeled similar peptide can be used as a surrogate of ^{90}Y PRRT to assess the biodistribution before therapy. ^{111}In emits 2 single γ -rays (173 and 247 keV) that can easily be imaged with an Anger camera; accurate quantification, however, remains cumbersome because attenuation and Compton scatter have to be taken into account in planar and SPECT images. Besides these physical limitations, labeling with ^{111}In instead of ^{90}Y is known to induce structural

changes in somatostatin analogs that affect the receptor-binding affinity and lead to significantly different biodistributions (14). The radiometal itself may also alter the pharmacokinetics, especially when the compound is metabolized. However, most of the kidney uptake is not somatostatin receptor-dependent, and, for example, ^{111}In -DOTATOC has proven useful—although not with perfect accuracy—at predicting the kidney toxicity in ^{90}Y -DOTATOC therapy (12,15).

Nevertheless, a dosimetry based on a more accurate ^{90}Y imaging acquisition, such as with PET, at the time of the first ^{90}Y PRRT cycle could have several benefits over ^{111}In SPECT. The benefits of ^{90}Y might include no need for extra amino acid infusion if ^{111}In SPECT is performed pretherapeutically or, alternatively, no ^{90}Y bremsstrahlung contamination using ^{111}In SPECT if performed simultaneously with the first ^{90}Y cycle; better prediction of tumor response, the uptake being receptor-dependent; improved dosimetry estimates because of the better spatial resolution and scatter correction obtained with PET than with SPECT studies; and no added radiation burden to the staff for ^{111}In studies.

Recently, despite the low positron branch of ^{90}Y ($3.2 \cdot 10^{-5}$) (16,17), dosimetry in liver selective internal radiotherapy (SIRT) by direct ^{90}Y time-of-flight (TOF) PET has proven feasible (18–20). The goal of the present study was to assess whether direct ^{90}Y PET of a first ^{90}Y PRRT cycle could also provide accurate dosimetry to optimize the injected activity of the following cycles. For this purpose, an anthropomorphic abdominal phantom was built, and images were acquired on a high-end lutetium yttrium orthosilicate (LYSO) TOF PET scanner and on a conventional bismuth germanate (BGO) scanner.

MATERIALS AND METHODS

Anthropomorphic Abdominal Phantom

The phantom consisted of an abdomen-shaped acrylic container filled with water (Fig. 1). Figure 2 shows the hand-made acrylic realization of the computational MIRD kidney phantom (21). Three vertebrae containing red marrow (RM) were also modeled. Two tumors were modeled by 7-mL hollow acrylic spheres and the spleen by a 250-mL plastic bag. Activities corresponded to a typical clinical situation (Supplemental Appendix A; supplemental materials are available online only at <http://jnm.snmjournals.org>).

Acquisition and Reconstruction

Eight scans (45-min acquisitions) in 3-dimensional mode were obtained on the Philips Gemini TF (LYSO) and Siemens Exact HR+ (BGO). Iterative reconstructions, with attenuation and scatter correction, were performed on each system (Supplemental Appendix B).

Renal Dosimetry Dependent on Cortex Geometry

A renal cortex volume of interest (VOI) was drawn by threshold on the CT scan slices, the threshold level being tuned to get the actual cortex volume of the phantom. A stylized number of decay (NDec) distributions, uniform inside the cortex VOI and null outside, was built to correspond to 1 M decays in the entire cortex VOI (Fig. 3). As previously validated for liver SIRT (20), a

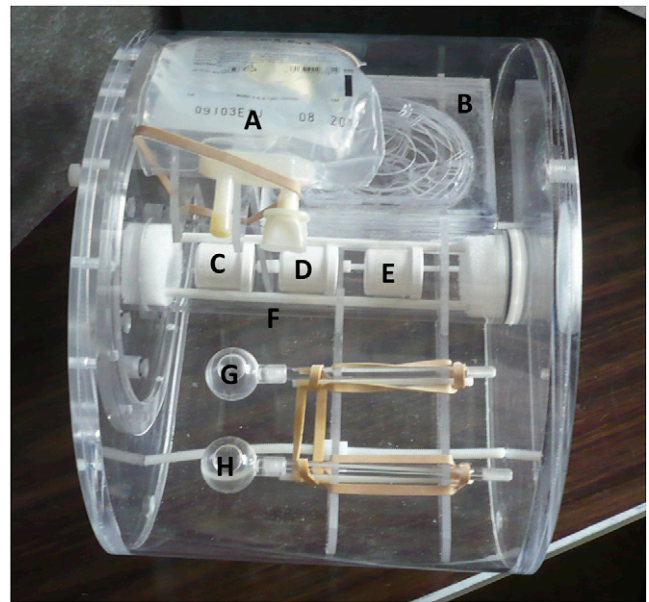


FIGURE 1. Upper oblique view of abdominal phantom before filling. (A) 250-mL plastic bag modeling spleen. (B) Phantom based on MIRD model of kidney (21). (C–E) 12-mL plastic bottle modeling RM in vertebra. (F) Acrylic cylinder containing vertebrae surrounded by K_2HPO_4 solution modeling bone attenuation. (G and H) Hollow 7-mL acrylic sphere modeling tumors. Transverse maximal section of phantom is 30×23 cm, and axial length is 22 cm.

regional dosimetry was calculated by convolution of this stylized NDec distribution with a ^{90}Y voxel S value kernel. The single kidney mean cortex-absorbed dose per unit cumulated activity in the cortex ($S_{\text{cortex} \leftarrow \text{cortex}}$ value) was measured as the mean value of this regional dosimetry inside the cortex VOI. Finally, the cortex mean-absorbed dose (MAD) was this measured $S_{\text{cortex} \leftarrow \text{cortex}}$ value multiplied by the NDec derived from the total cortex activity, $A(t)$, measured on the reconstructed distribution activity:

$$\text{NDec} = \int_0^{+\infty} A(t) dt. \quad \text{Eq. 1}$$

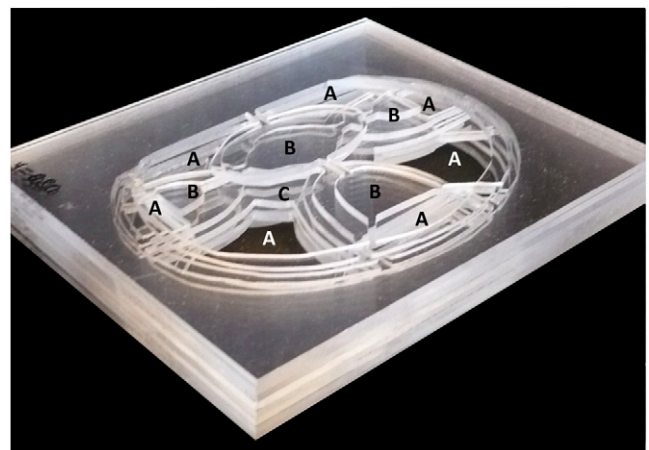


FIGURE 2. Nine central 2-mm-thick acrylic coronal slices constituting MIRD fillable kidney phantom model (21). Renal cortex is modeled by empty spaces (A) to be filled with activity; medullary pyramids (B) and renal pelvis (C) are devoid of activity.

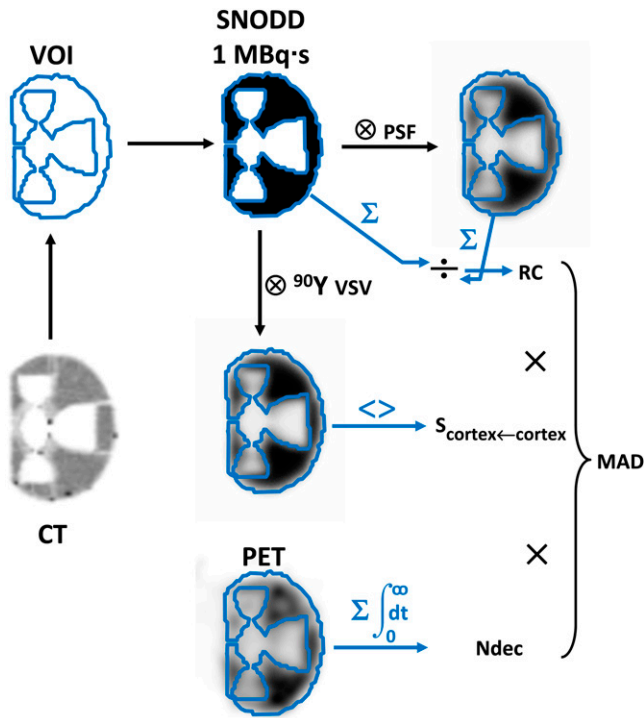


FIGURE 3. Schematic diagram of MAD computation. After cortex VOI was drawn, a synthetic NDec distribution (SNODD) corresponding to 1 MBq·s decays in cortex was built and convolved with PET PSF to obtain cortex RC. $S_{\text{cortex} \leftarrow \text{cortex}}$ value is mean value of cortex VOI applied on convolution of SNODD by ^{90}Y voxel S value. Product of these 2 quantities multiplied by NDec in cortex VOI provided by Equation 1 gives cortex MAD. Blue arrows emphasize that summation or averaging is limited to cortex VOI. VSV = voxel S value.

In our phantom model without biologic washout, Equation 1 gives:

$$\text{NDec} = A(0) \times (64.2 \times 3,600 / \ln(2)), \quad \text{Eq. 2}$$

where $A(0)$ is expressed in becquerels, and 64.2 is the physical half-life of ^{90}Y in hours. The obtained MAD was further corrected using a spatial resolution recovery coefficient (RC) (20). The actual MAD was the $S_{\text{cortex} \leftarrow \text{cortex}}$ value (given in MIRD pamphlet no. 19 (21)) rescaled for the cortex VOI multiplied by the NDec corresponding to twice the actual cortex activity (because the MIRD formalism provides the S value for both kidneys).

Cortex RC

A second cortex distribution was derived by convolving the stylized NDec distribution with the point-spread function (PSF) of the whole tomographic process. The RC was measured as the ratio of the total NDecs in the cortex VOI of the raw and of the convoluted stylized NDec distribution (Fig. 3). The PSF was approximated using a gaussian function, with a full width at half maximum (FWHM) that was measured on a similarly reconstructed ^{22}Na (2 MBq) point source (1-min acquisition in air), providing 2.5-M counts.

Tumors and RM Dosimetry

Tumors and RM dosimetry were computed using previously validated simple standard methods (Supplemental Appendix C).

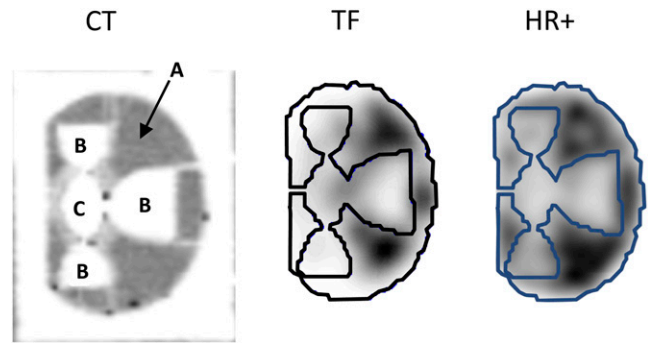


FIGURE 4. Coronal slices of kidney based on the MIRD fillable kidney phantom model (21), obtained by averaging reconstructions of eight 45-min acquisitions for Gemini TF (TF) and Exact HR+ (HR+) systems. (A) Renal cortex. (B) Medullar pyramids. (C) Renal pelvis. There is lack of reconstructed activity on kidney (left side facing spine) for Gemini TF reconstruction.

RESULTS

The full width at half maximum was 9.0 mm for the Exact HR+ and 9.4 mm for the Gemini TF reconstruction, giving cortex RC values of 1.53 and 1.60, respectively. The measured volume of the phantom cortex was 107 mL. Compared with the expected 100.75 mL reported in MIRD pamphlet no. 19 (21), this measured volume corresponds to an average error of about 0.6 mm on the cutting edges. The experimentally derived single-kidney $S_{\text{cortex} \leftarrow \text{cortex}}$ value, expressed in $\text{mGy} \cdot \text{MBq}^{-1} \cdot \text{s}^{-1}$, was $2 \times 5.66 \cdot 10^{-4}$, representing a relative deviation of -4% from the value obtained from MIRD pamphlet no. 19 (21) after rescaling to 107 mL ($2 \times 5.91 \cdot 10^{-4}$). This rescaled S value multiplied by the NDec obtained using Equation 2 gave an actual cortex MAD of 13.80 Gy. Figure 4 shows CT and PET partial coronal slices of each compartment; Figure 5 shows a maximum-intensity-projection (MIP) view of the phantom. Table 1 shows the renal cortex MADs and Table 2 the MADs for the tumors and RM derived from the different reconstructions. As a result of the lower sensitivity of

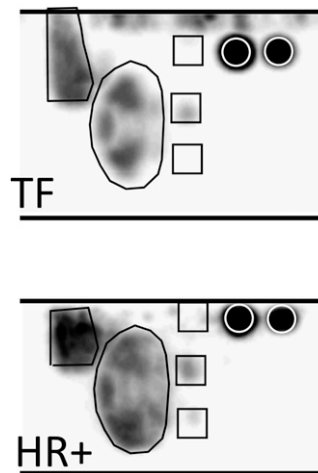


FIGURE 5. Maximum-intensity-projection views of abdominal phantom obtained by averaging reconstructions of eight 45-min acquisitions for Gemini TF (TF) and Exact HR+ (HR+) systems. Horizontal lines represent limits of axial field of view. Only central vertebra is visible in Gemini TF reconstruction.

TABLE 1
Cortex MAD for Eight 45-Minute Acquisitions

Acquisition no.	LYSO Gemini TF		BGO Exact HR+	
	MAD (Gy)	Relative deviation (%)	MAD (Gy)	Relative deviation (%)
1	11.47	-16.91	12.65	-8.31
2	11.09	-19.67	13.52	-2.04
3	11.70	-15.26	13.59	-1.52
4	11.71	-15.16	13.29	-3.69
5	11.67	-15.47	13.98	1.26
6	11.66	-15.51	13.24	-4.10
7	10.74	-22.21	13.67	-0.95
8	10.53	-23.74	13.30	-3.62
Average ± SD	11.32 ± 0.47	-17.99	13.41 ± 0.39	-2.87

Relative deviation is computed vs. value obtained using MIRD pamphlet no. 19 (21), rescaled by cortex volume ratio (i.e., true = 13.80 Gy).

the 3-dimensional-mode acquisition in these regions (data not shown), large statistical uncertainty affected the MAD found for the 2 external vertebrae.

DISCUSSION

The following are the 4 major steps of the renal dosimetry method proposed (Fig. 3):

1. Delineate the cortex VOI on the CT scan, and generate a stylized NDec distribution.
2. Determine the cortex RC by convolving the stylized NDec distribution with the final PSF of the PET system.
3. Compute the single-kidney $S_{\text{cortex} \leftarrow \text{cortex}}$ value by averaging the regional dosimetry obtained after convolving the stylized NDec distribution with a ^{90}Y voxel S value kernel.
4. Assess the total reconstructed activity in the cortex VOI.

The proposed method takes into account the 2 major effects induced by individual patient variations in cortex geometry as determined from step 1: the loss in reconstructed counts due to the finite spatial resolution of the imaging system (step 2) and the loss in energy deposit due to the β^- range of the radioisotope (step 3). The method was especially designed to overcome the usual amplification of the statistical uncertainty by the spatial resolution–recovery

process (Supplemental Appendix D). The proposed method allows the nonuniform uptake of the renal cortex in ^{90}Y PRRT, as observed in humans by ex vivo autoradiography (22), to be taken into account. This could be achieved by building the stylized NDec distribution according to the model of 3-dimensional activity distribution in the renal cortex developed by Konijnenberg et al. (23).

The $S_{\text{cortex} \leftarrow \text{cortex}}$ value obtained here agreed well with the value reported in MIRD pamphlet no. 19 (21). To our knowledge, ours is the first study to validate the possibility of using experimental data (i.e., the CT cortex VOI) to retrieve the pure computational value obtained by Monte Carlo from geometric equations.

Cortex MADs obtained with the conventional BGO system (Exact HR+) were more accurate than those obtained with the state-of-the-art LYSO TOF system (Gemini TF), contradicting the results of our phantom study with ^{90}Y SIRT, which compared different PET systems (van Elmbt et al., unpublished data, 2010). We hypothesize that in liver SIRT, the BGO system, with its larger time coincidence window and its longer crystal afterglow, strongly suffered from the high activity present in the field of view (1.5 GBq in the whole liver), providing a high random coincidence rate. The specific activity of the tumors modeled in the liver SIRT phantom was about 10 times higher than the renal cortex activity modeled here. As a result, in the present low-counting-rate study, each LYSO crystal

TABLE 2
Average ± SD of MAD for Tumors (T1, T2) and Central Vertebra (V2) Obtained from Eight 45-Minute Acquisitions

Compartment	True MAD (Gy)	Gemini TF		Exact HR+	
		MAD (Gy)	Relative deviation* (%)	MAD (Gy)	Relative deviation* (%)
T1 < h >	157.3	166.8 ± 21.0	6.0	146.1 ± 8.9	-7.1
T2 < h >	69.2	71.6 ± 11.9	3.4	62.8 ± 8.9	-9.2
V2 < h >	2.0	0.7 ± 0.3	-64.0	1.2 ± 0.2	-40.0

*Relative deviation with true absorbed dose.

became affected by a lower ratio of the counts coming from the phantom than from the natural radioactivity of the crystal (i.e., contaminant ^{176}Lu). The lower renal cortex activity modeled in our study is clearly visible on the coronal cortex slice (Fig. 4), on which the activity in the region facing the spine, undergoing the maximal attenuation, is almost completely missing in the Gemini TF reconstruction.

The accuracy to determine the renal cortex-absorbed dose with the BGO PET system was excellent (mean error, 3%). Despite the low positron branching of ^{90}Y , it was shown that the sensitivities of ^{90}Y PET and bremsstrahlung SPECT were similar (24). The small SD of renal-absorbed dose estimates showed that the statistics are adequate (Table 1). Nevertheless, it is anticipated that such a result may not be achieved in clinical applications. The additional limitations inherent to studies in humans are the difficulty in exactly delineating the renal cortex, even with intravenous iodinated contrast; possible patient motion between the PET and CT acquisitions, resulting in misalignment of the cortex VOI on the PET image; need to assess the biologic washout from a limited number of time points; and reduction in counting rate from the late-time-point acquisition due to biologic washout and physical decay. Compared with our phantom comprising a single kidney, the additional noise resulting from the lower statistics can be reduced by averaging the MAD of both kidneys, at least in patients having a symmetric kidney function. The alignment of the CT-determined renal cortex VOI on the PET scan should be especially critical on conventional PET scanners—that is, those without a CT component. In this case, the acquisition of an additional 5-min scan just after injection of approximately 30 MBq of ^{18}F -FDG, without moving the patient and table, may be advisable. The acquisition of a scan just after injection will provide a good-quality image of the kidneys to compute the alignment parameters, using a 2-step procedure.

As expected, both systems obtained a good result for the tumors with a higher specific activity. Neither PET system was able to get accurate results for the RM.

CONCLUSION

The accurate estimation of the MADs of the renal cortex and tumors obtained from ^{90}Y PET in the anthropomorphic phantom supports the feasibility of direct tumor and renal dosimetry in ^{90}Y PRRT by direct ^{90}Y PET after the first PRRT cycle. This possibility is especially true when crystals that do not contain natural radioactive material, such as BGO or gadolinium silicate (GSO), are used.

REFERENCES

- Brans B, Linden O, Giammarile F, Tennvall J, Punt C. Clinical applications of newer radionuclide therapies. *Eur J Cancer*. 2006;42:994–1003.
- de Jong M, Breeman WA, Valkema R, Bernard BF, Krenning EP. Combination radionuclide therapy using ^{177}Lu - and ^{90}Y -labeled somatostatin analogs. *J Nucl Med*. 2005;46(suppl 1):13S–17S.
- Barone R, Borson-Chazot F, Valkema R, et al. Patient-specific dosimetry in predicting renal toxicity with ^{90}Y -DOTATOC: relevance of kidney volume and dose rate in finding a dose-effect relationship. *J Nucl Med*. 2005;46(suppl 1):99S–106S.
- Pauwels S, Barone R, Walrand S, et al. Practical dosimetry of peptide receptor radionuclide therapy with ^{90}Y -labeled somatostatin analogs. *J Nucl Med*. 2005;46(suppl 1):92S–98S.
- Flux G, Bardies M, Monsieurs M, Savolainen S, Strand SE, Lassmann M. The impact of PET and SPECT on dosimetry for targeted radionuclide therapy. *Z Med Phys*. 2006;16:47–59.
- Flux G, Bardies M, Chiesa C, et al. Clinical radionuclide therapy dosimetry: the quest for the “Holy Gray.” *Eur J Nucl Med Mol Imaging*. 2007;34:1699–1700.
- Brans B, Bodei L, Giammarile F, et al. Clinical radionuclide therapy dosimetry: the quest for the “Holy Gray.” *Eur J Nucl Med Mol Imaging*. 2007;34:772–786.
- Sgouros G, Frey E, Wahl R, et al. Three-dimensional imaging-based radiobiological dosimetry. *Semin Nucl Med*. 2008;38:321–334.
- Stabin MG, Brill AB. State of the art in nuclear medicine dose assessment. *Semin Nucl Med*. 2008;38:308–320.
- Minarik D, Gleisner KS, Ljungberg M. Evaluation of quantitative Y-90 SPECT based on experimental phantom studies. *Phys Med Biol*. 2008;53:5689–5703.
- Sgouros G. Yttrium-90 biodistribution by yttrium-87 imaging: a theoretical feasibility analysis. *Med Phys*. 1998;25:1487–1490.
- Wessels BW, Konijnenberg MW, Dale RG, et al. MIRD pamphlet no. 20: the effect of model assumptions on kidney dosimetry and response—implications for radionuclide therapy. *J Nucl Med*. 2008;49:1884–1899.
- Walrand S, Jamar F, Mathieu I, et al. Quantitation in PET using isotopes emitting prompt single gammas: application to yttrium-86. *Eur J Nucl Med Mol Imaging*. 2003;30:354–361.
- de Jong M, Bakker WH, Krenning EP, et al. Yttrium-90 and indium-111 labelling, receptor binding and biodistribution of [DOTA0,0-Phel,Tyr3]octreotide, a promising somatostatin analogue for radionuclide therapy. *Eur J Nucl Med*. 1997;24:368–371.
- Cremonesi M, Ferrari M, Bodei L, Tosi G, Paganelli G. Dosimetry in peptide radionuclide receptor therapy: a review. *J Nucl Med*. 2006;47:1467–1475.
- Ford K. Predicted 0+ level of Zr90. *Phys Rev*. 1955;98:1516.
- Nickles RJ, Roberts AD, Nye JA, et al. Assaying and PET imaging of yttrium-90: $1 >> 34\text{ppm} > 0$. *IEEE Nucl Sci Symp Rec*. 2004;6:3412–3414.
- Lhommel R, Goffette P, Van den Eynde M, et al. Yttrium-90 TOF PET scan demonstrates high-resolution biodistribution after liver SIRT. *Eur J Nucl Med Mol Imaging*. 2009;36:1696.
- Werner MK, Brechtel K, Beyer T, Dittmann K, Pfannenbergs C, Kupferschläger J. PET/CT for the assessment and quantification of ^{90}Y biodistribution after selective internal radiotherapy (SIRT) of liver metastases. *Eur J Nucl Med Mol Imaging*. 2009;37:407–408.
- Lhommel R, van Elmbt L, Goffette P, Van et al. Feasibility of yttrium-90 TOF-PET based dosimetry in liver metastasis therapy using SIR-spheres. *Eur J Nucl Med Mol Imaging*. 2010;37:1654–1662.
- Bouchet LG, Bolch WE, Blanco HP, et al. MIRD pamphlet no. 19: absorbed fractions and radionuclide S values for six age-dependent multiregion models of the kidney. *J Nucl Med*. 2003;44:1113–1147.
- De Jong M, Valkema R, Van Gameren A, et al. Inhomogeneous localization of radioactivity in the human kidney after injection of [^{111}In -DTPA]octreotide. *J Nucl Med*. 2004;45:1168–1171.
- Konijnenberg M, Melis M, Valkema R, Krenning E, de Jong M. Radiation dose distribution in human kidneys by octreotides in peptide receptor radionuclide therapy. *J Nucl Med*. 2007;48:134–142.
- Rault E, Clementel E, Vandenberghe S, et al. Comparison of yttrium-90 SPECT and PET images [abstract]. *J Nucl Med*. 2010;51(suppl 2):125.